77-GT-37

Printed in U.S.A.

an ASME publication

$3.00 PER COPY
$1.50 TO ASME MEMBERS

Experimental Investigations of Supersonic Cascades Designed for High Static Pressure Ratios

R. FUCHS

H. STARKEN

Deutsche Forschungs- und Versuchsanstalt
für Luft- und Raumfahrt E.V.,
Institute für Luftstrahlantriebe,
Linder Höhe, Köln, Germany

The outlet conditions of supersonic compressor rotors designed for very high total pressure ratios can be highly supersonic (impulse rotors). Then the following stator blade row has to build up high static pressure ratios at supersonic inlet conditions. This paper describes part of a research work which should answer, if it is at all possible to realize such high static pressure ratios in a cascade. Cascades with convergent-divergent blade passages were designed and optimized by boundary layer calculations. In a first step no flow turning was incorporated in the blade sections. A three-shock-type cascade was found to be an optimum design. The wind tunnel measurements resulted in static pressure ratios of the order of 6 and total pressure ratios of 0.77 at inlet Mach numbers of 2.2. In a second step the flow turning to axial direction was realized. For that two types of cascades were built and tested. One was a tandem type cascade and the other a single row cascade. The experiments at inlet design conditions resulted in static pressure ratios of the order of 6.5 and total pressure ratios of 0.72.

Contributed by the Gas Turbine Division of The American Society of Mechanical Engineers for presentation at the Gas Turbine Conference & Products Show, Philadelphia, PA, March 27-31, 1977. Manuscript received at ASME Headquarters December 15, 1976.

Copies will be available until December 1, 1977.

Experimental Investigations of Supersonic Cascades Designed for High Static Pressure Ratios

R. FUCHS H. STARKEN

INTRODUCTION

Theoretical considerations for supersonic compressors indicated possible high stage pressure ratios for the impulse rotor and shock-in-stator type compressor stage (1).[1] In this case, the impulse type rotor has to be designed for high energy input by large flow turnings. The static pressure rise is very moderate or even zero. Only the stator converts the kinetic energy into static pressure. Therefore, the rotor outlet flow enters the stator at supersonic velocities. The stator flow is then decelerated to subsonic velocities and turned to axial direction.

The shock-in-stator stage might also be preferable in view of the control of shock-induced flow separation. Another reason for a look at the impulse type compressor is that especially the impulse rotors showed some encouraging results (2-5). But as shown by the review paper of Klapproth (6), the stage performances in all cases were unsatisfactory, probably caused by the following stator (7, 8).

Reference (6) gives an explanation by showing that the total pressure recoveries of all tested stators were lower than normal shock recovery and drop rapidly with increasing inlet Mach number.

From this state-of-the-art, the presented cascade investigation started. The aim was to design a stator cascade for a high inlet Mach number ($M \geq 2$) which should reach a total pressure recovery higher than obtainable by a normal shock wave.

From the rotor results of Reference (5) and Table 1 of Reference (6), as well as from theoretical considerations, it follows that for suitable stator inlet angles the axial outlet Mach number of the rotor must be supersonic. This has to be considered in the stator cascade design.

If rotor and stator are not correctly matched, it may happen that the rotor is throttled too much by the stator. In this case, the design supersonic flow in the rotor cannot be started.

[1] Numbers in parentheses designate References at end of paper.

NOMENCLATURE

- l = chord length
- M = Mach number
- p = static pressure
- p_t = total pressure
- t = pitch
- x = coordinate from the leading edge in chord direction
- b = cascade overlapping (tandem cascade)
- d = trailing edge-leading edge distance (tandem cascade)
- AVR = axial velocity-density ratio
- β = flow angle (measured against cascade front)
- β_s = stagger angle (measured against cascade front)

Suffixes

- 1 = uniform inlet conditions
- 2 = uniform outlet conditions
- PS = pressure surface
- SS = suction surface
- A = first cascade of a tandem cascade
- B = second cascade of a tandem cascade

It may be that this was also a reason for the unsatisfactory stage results achieved in the past. The unthrottled test results showed this failure. In order to overcome this problem, the stator blades must be movable.

CASCADE WITHOUT TURNING

Cascade Design

A very simple way to decelerate a supersonic flow is that by normal shock wave. But the total pressure losses caused by a normal shock are increasing rapidly with Mach number. Fig. 1 shows the total pressure ratios for Mach numbers from 1.0 to 2.8.

For upstream Mach numbers greater than 2.0, which was our design goal, the resulting total pressure ratios are lower than 0.72. To make the thing worse, the shock-boundary layer-interactions will cause separation for upstream Mach numbers higher than 1.3. The separation causes higher losses and the real total pressure ratio will be even lower than the theoretical one.

For cascades which decelerate the flow from high supersonic velocities to subsonic velocities, the aim must therefore be to reduce the total pressure losses caused by shock waves and boundary layer separations. In order to reduce the high losses caused by a single normal shock, one possibility is to decelerate the flow by several oblique shock waves or even an isentropic compression as suggested by Oswatitsch (9).

This method has been applied successfully for supersonic intakes. The static pressure ratios of the multiple shock system can be designed in such a way that no boundary layer separation should be expected.

In order to apply this method to supersonic cascades, one has to keep in mind the periodicity requirement and the design conditions caused by the axial supersonic inlet flow. From both, it follows, as has been shown in Reference (10), that the first oblique shock wave must run into the blade passages or, as a limiting condition, may be positioned just in the cascade front.

A computer program for the design of an optimum cascade has been developed. The supersonic part of the flow was computed by the method of characteristics and the boundary layer by the integral method of Walz (11). At the loci where the shock interacts with the boundary layer, the method of Walz failed because of the high pressure gradients in the main stream. Therefore, a subroutine based on the method of Reshotko and Tucker (12) was used. For a design-inlet-Mach number of 2.0, several types of cascades were computed. Promising results were obtained with the 3-shock-type-cascade of Fig. 2.

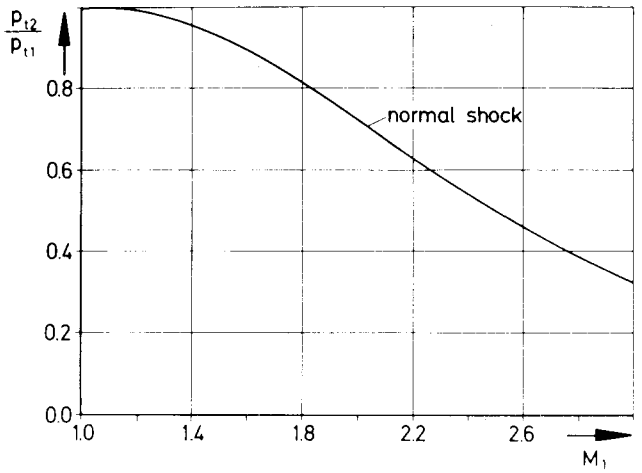

Fig. 1 Total pressure ratio of a normal shock as function of the upstream Mach number

In order to simplify the first phase of the project, no overall flow deviation was incorporated in the first design. The inlet Mach number is reduced by two oblique shocks from 2.0 down to 1.3 at the cascade throat. As before, the first oblique shock is placed just in the front of the cascade. This case was chosen as the design condition, because then no double shock system does occur at the pressure side. The second oblique shock runs into the blade passage. A reflection on the suction side is prevented by bending the suction side at the interaction point.

The normal shock is positioned as much upstream as a stable position is possible; that means just downstream of the throat. Therefore the Mach number in front of the normal shock is only slightly higher than 1.3. Behind the normal shock, a subsonic diffusion is obtained in the divergent part of the cascade passage.

Experimental Results

The design cross-section-ratio from inlet to throat of the cascade fulfilled the theoretical starting criterium of Kantrowitz, Donaldson (13) and Eggink (14). However, in the cascade wind tunnel experiments, the inlet Mach number had to be increased to start the supersonic flow. After starting had been

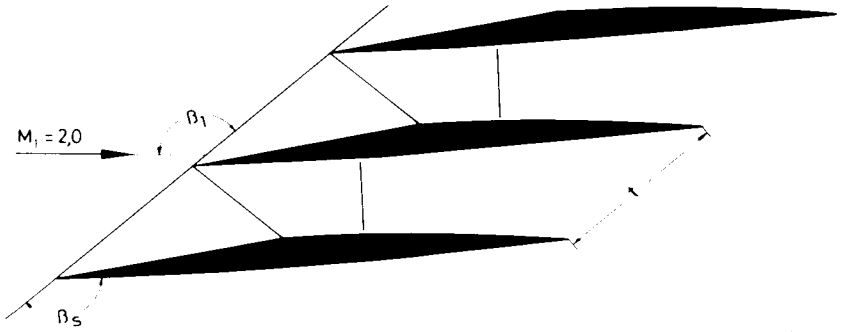

Fig. 2 Supersonic Cascade DFVLR-SAV 16. Design data: $M_1 = 2.0$, $\beta_1 = 139$ deg, $\beta_s = 144$ deg, $t/l = 0.348$

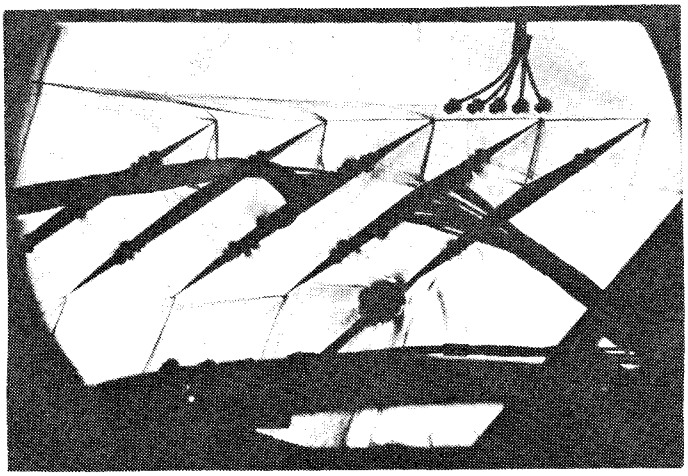

Fig. 3 Schlieren picture of started but unthrottled supersonic cascade $M_1 = 2.18$

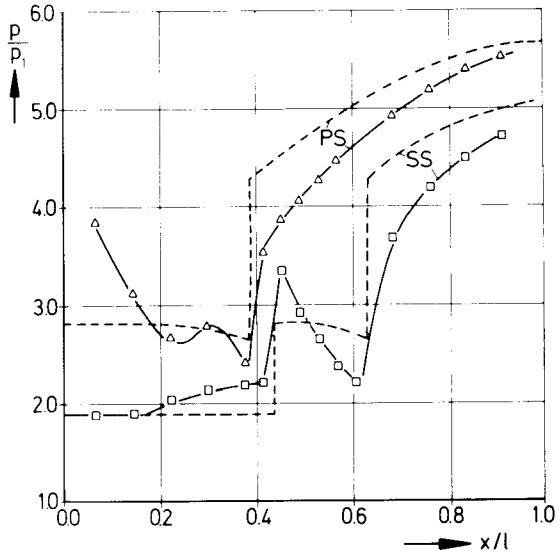

Fig. 4 Static pressure distribution on pressure and suction side, maximum throttling. $M_1 = 2.2$; $\beta_1 = 139$ deg. --- computed ____ measured

achieved at a Mach number of about 2.3, the inlet Mach number could not be decreased enough to reach the design value of 2.0.

The lowest possible inlet Mach number reached in the tests was between 2.1 and 2.2. At the minimum Mach number, the position of the first oblique shock wave was already in the cascade front (Fig. 3). It seems that the effective wedge angle at the profile leading edge was about 2.5 deg larger than the metal angle.

Insufficient boundary layer correction at the leading edge may be one possible reason. A second one may be the profile-side wall-wedge effects. But even more important was the throttling behavior of the started cascade. By increasing the back pressure above a certain relatively low value, the supersonic flow broke down; the normal shock being far away from its design position.

To avoid this upstream reaction, the sidewall boundary layers had to be reduced. Therefore the experimental setup was changed. Additional metal sidewalls were built inside parallel to the wind-tunnel windows and in order to stabilize the subsonic flow metal wedges were added on both the sidewalls, resulting in a streamtube contraction. Without this contraction, the axial velocity density ratio varied considerably from test to test.

However, no Schlieren visualization of the blade passages were possible under these conditions. The shock positions could only be observed by a mercury-manometer-battery which showed the static pressure distribution inside the profile passage. Along midspan of

suction and pressure side of two adjacent blades, 15 static pressure holes showed whether the design shock pattern were realized or not.

As a result of this modification of the test section, the back pressure of the cascade could be changed easily between the unthrottled case and the maximum design value.

An example for the measured profile pressure distribution is shown in Fig. 4. The dotted line is the design pressure distribution at the new inlet Mach number $M_1 = 2.2$. From the measured distribution, it can be concluded that the normal shock wave is in the design position, which is the maximum throttled case. The design and the measured distributions are similar but there are certain discrepancies at the shock-boundary-layer interaction points.

The total pressure p_{t2} at the cascade outlet was measured at midspan by a traversing pitot tube. The static pressures p_1 and p_2 at inlet and outlet of the cascade were taken from static pressure holes on the sidewalls. The outlet flow angle β_2 was measured by a conventional three-hole-probe. The inlet flow angle β_1 is prescribed by the cascade setting in the wind tunnel, because at supersonic axial velocities no unique incidence condition is valid. The inlet flow angle could be changed by rotatable wind tunnel side walls. Mean values are derived from the test data of the measuring planes. The data reduction procedure is described in Reference (15). In the diagram of this paper, mass averaged values are presented.

In Fig. 5, total and static pressure ratios are presented for the design inlet flow angle $\beta_1 = 139$ deg and three different inlet Mach numbers but all at maximum back pressure. High, total pressure ratios were obtained at low, minimum total pressure ratios at high Mach numbers. In order to show the advantages of the new cascade design, the theoretical pressure ratio for a normal shock is also drawn in Fig. 5. It can be seen that compared with a single normal shock, there is considerable gain in total pressure when decelerating the flow by a multiple-shock cascade.

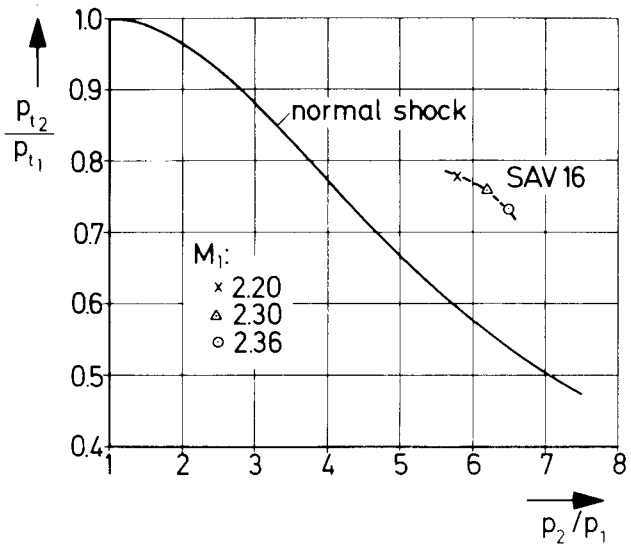

Fig. 5 Total pressure ratio of the tested cascade at three different inlet Mach numbers and at maximum back pressure compared with normal shock relation

CASCADES WITH FLOW TURNING

In order to use the described cascade for a stator blade row behind an impulse-type rotor, a flow turning to about axial direction has to be achieved. For this purpose, two types of cascades were built and tested. One of them was a tandem type cascade and the other one was a single row cascade. The main reason for the tandem cascade was the existence of a suitable high turning MCA blade section which could be used easily as subsonic part of the cascade.

Tandem Cascade

The first row of the tandem cascade is the three-shock-type-cascade SAV 16 previously described. The second row is a cascade of MCA (multiple circular arc) profiles with a turning of 49 deg (Fig. 6).

The wind tunnel tests offered no real problems in starting the cascade. Fig. 7 shows a Schlieren picture of the completely supersonic flow throughout the cascade.

But again, the additional inner metal-sidewalls parallel to the windows had to be installed in order to establish the design normal shock position. However, there was a second reason to use the metal-sidewalls. Because the high-turning angle would result in a much too high subsonic deceleration, the flow cross sections downstream of the throat had to be reduced. This was done by adding metal wedges on both the sidewalls.

The mass averaged mean values of total and static pressure ratio are presented in Fig. 8. These are results for an inlet flow angle of $\beta_1 = 139$ deg, three different inlet Mach numbers but always at optimum back pressure. Again, the lowest Mach number belongs to the measuring point with the highest total but lowest static pressure ratio and the high-

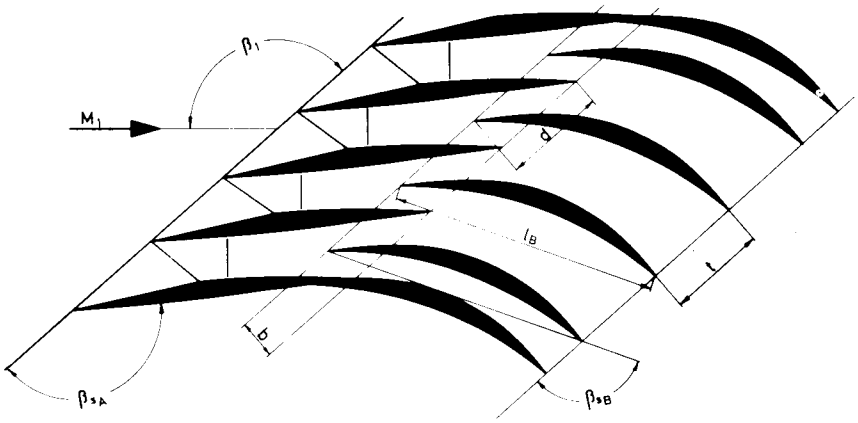

Fig. 6 Supersonic DFVLR-tandem cascade with turning to axial direction. $M_1 = 2.0$; $\beta_1 = 139$ deg; $\beta_{sA} = 144$ deg; $t/l_A = 0.348$; $\beta_{sB} = 120.5$ deg; $t/l_B = 0.362$; b = 18 mm; d = 48 mm

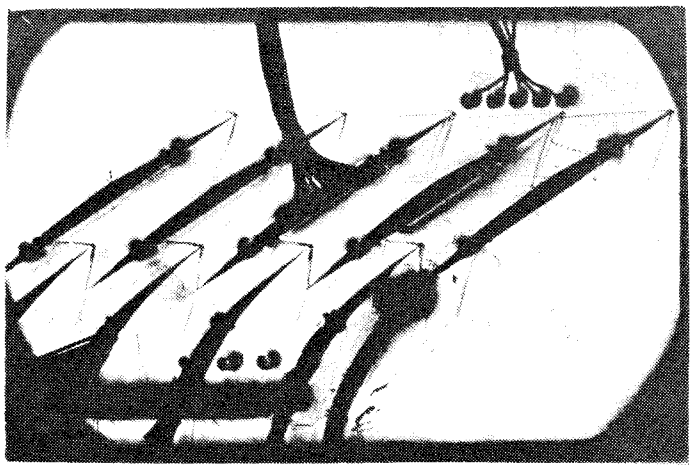

Fig. 7 Schlieren picture of started but unthrottled tandem-type cascade. $M_1 = 2.3$; $\beta_1 = 139$ deg

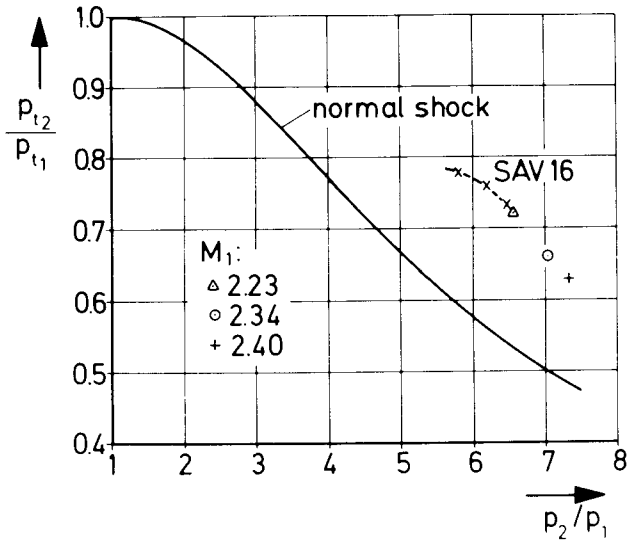

Fig. 8 Total pressure ratio of tandem type and single row cascade without turning. $\beta_1 = 139$ deg

est Mach number belongs to the lowest total but highest static pressure ratio.

As can be seen from Fig. 8, the total pressure ratio results are remarkably better than the normal shock relation at the same static pressure ratio. In comparison to the results of the cascade without turning for the same inlet Mach number, the total pressure ratio is worse but the static pressure ratio is higher.

Single Row Cascade

The single row type cascade with flow turning is designed such that it corresponds in its front part to the cascade without turning. The subsonic part is shaped parabolically to turn the flow to axial direction. This area must not show a throat section (Fig. 9).

During the wind tunnel tests, again no starting problems occurred (Fig. 10). The starting behavior of this cascade was even better than that of the tandem type cascade. Again, the additional inner metal sidewalls with wedges had to be installed to be able to throttle the cascade and to lower the pressure rise caused by the high turning.

The mass averaged mean values of total pressure ratio and static pressure ratio are

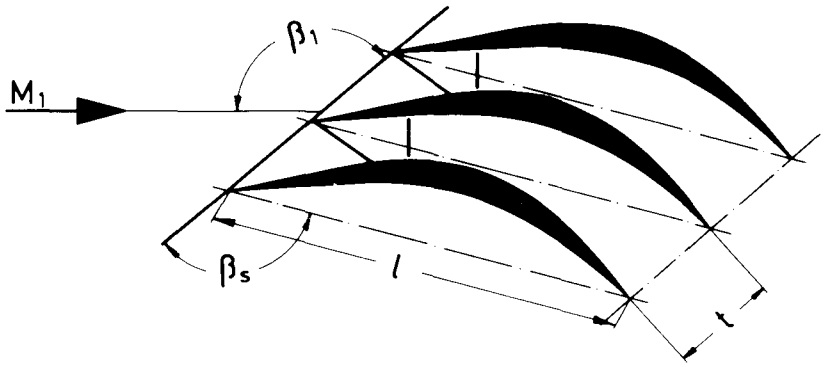

Fig. 9 Supersonic cascade DFVLR-SAV 21 with turning to axial direction. $M_1 = 2.0$; $\beta_1 = 139$ deg; $\beta_s = 125$ deg; $t/l = 0.26$

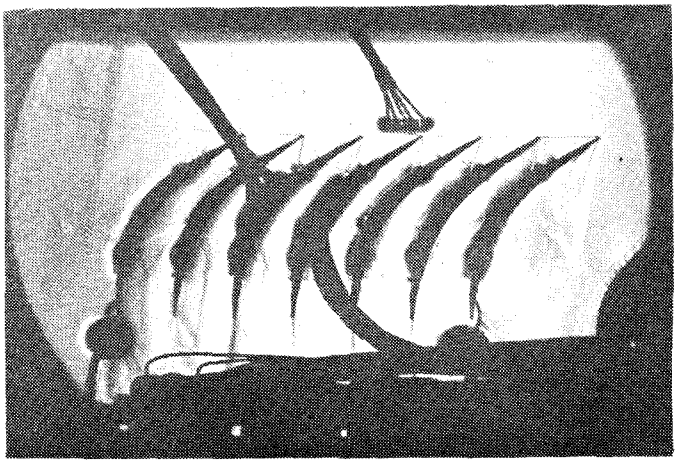

Fig. 10 Schlieren picture of started but unthrottled single row type cascade. $M_1 = 2.2$; $\beta_1 = 139$ deg

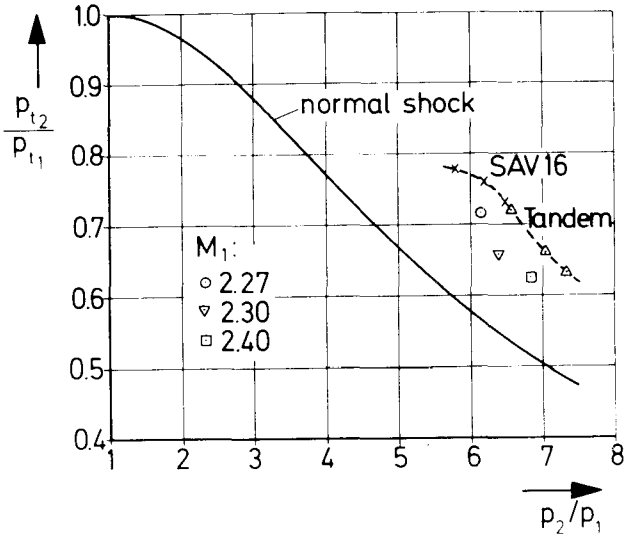

Fig. 11 Total pressure ratio of single row cascade with and without turning, and of tandem type cascade $\beta_1 = 139$ deg

presented in Fig. 11. These are again results for an inlet flow angle of $\beta_1 = 139$ deg, three different inlet Mach numbers and optimum back pressure. The lowest inlet Mach number belongs to the result point of the highest total pressure ratio and lowest static pressure ratio and vice versa.

It follows from Fig. 11 that the results are always better than for a normal shock at the same static pressure ratio. In comparison to the tandem type cascade, the results are slightly worse because at equal inlet Mach numbers the total pressure ratio is the same, but the static pressure ratio is smaller.

CONCLUSIONS

The subject of this paper was to answer the question if it is possible to convert the high total pressure, for instance, behind an impulse-type rotor, into high static pressure and how large would be the associated total pressure losses.

Three different cascades of the 3-shock type were designed and tested at an inlet Mach number of $M_1 = 2.2$ and an inlet flow angle $\beta_1 = 139$ deg. The results are:

In all three cascades, it was possible to obtain a high static pressure ratio between 5.7 and 6.5.

The two cascades with flow turning to axial direction achieved higher static pressure ratios than the cascade without flow turning.

The static pressure ratio of the tandem

type cascade was slightly higher than that of the single row turning cascade.

The total pressure ratios of all three cascades (0.77-0.72) were remarkably higher than those of a single normal shock at equal static pressure ratios.

The total pressure ratio of the cascade without flow turning was higher than those of the cascades with turning.

The total pressure ratios of the two cascades with turning were equal.

The starting behavior of the single row turning cascades was better than that of the tandem cascade.

As would be expected, there are certain difficulties to start the supersonic flow at the high area contraction ratios inherent in the cascade design. Because in a compressor it is not as easy as in the wind tunnel to increase the stator inlet Mach number, variable stator blades might be required there.

In order to start the axial supersonic flow in the exit of an impulse type rotor, it would be necessary in any case to use a variable stator blade row.

It is intended to investigate this in the near future by testing a variable blade section of the SAV 21 type in a rotating machine. Some preliminary work on a variable cascade has already been performed.

REFERENCES

1 Wright, L. C., and Klapproth, J. F., "Performance of Supersonic Axial-Flow Compressors Based on One-Dimensional Analysis," NACA RM E8L10, Mar. 1949.

2 Tysl, E., Klapproth, J., and Hartmann, M., "Investigation of a Supersonic-Compressor Rotor With Turning to Axial Direction. I-Rotor Design and Performance," NACA RM E 53F23, Aug. 1953.

3 Wilcox, W. W., "Investigation of Impulse-Type Supersonic Compressor With Hub-Tip Ratio of 0.6 and Turning to Axial Direction. I-Performance of Rotor Alone," NACA RM E 54B25, May 1954.

4 Goldberg, Th., and Erwin, J., "Performance of an Impulse-Type Supersonic-Compressor Rotor Having a Mean Turning of 114 deg," NACA RM L 56J01, Jan. 7, 1957.

5 Simon, H., "Anwendung verschiedener Berechnungsverfahren zur Auslegung eines Oberschallverdichter-Laufrades und dessen experimentelle Untersuchung," Diss.TH Aachen, Nov. 1973.

6 Klapproth, J. F., "A Review of Supersonic Compressor Development," Transactions of ASME, Series A, Journal of Engineering for Power, Vol. 83, No. 3, July 1961, p. 258.

7 Klapproth, J. F., Ullman, G. N., and Tysl, E. R., "Performance of an Impulse-Type Supersonic Compressor With Stators," NACA RM E 52B22, Apr. 1952.

8 Wilcox, W. W., "Investigation of Impulse-Type Supersonic Compresssor With Hub-Tip Ratio of 0.6 and Turning to Axial Direction. II - Stage Performance With Three Sets of Stators," NACA RM E 55F28, 1955.

9 Oswatitsch, K., "Der Druckrückgewinn bei Geschossen mit Rückstossantrieb bie hohen Oberschallgeschwindigkeiten," (Nachdruck) DVL-Bericht Nr. 49, 1957.

10 Starken, H., and Lichtfuss, H. J., "Supersonic Cascade Performance," AGARD Lecture Series 39, Brüssel und Kongsberg (Norwegen), June 1970.

11 Walz, A., "Strömungs- und Temperaturgrenzschichten," Verlag G. Braun, Karlsruhe, 1966.

12 Reshotko, E., and Tucker, M., "Effect of a Discontinuity on Turbulent Boundary-Layer-Thickness. Parameters with Application to Shock-Induced Separation," NACA-TN 3454, 1955.

13 Kantrowitz, A., and Donaldson, C., "Preliminary Investigation of Supersonic Diffusers," NACA ACR No. L5D20, 1945.

14 Eggink, H., "Strömungsaufbau und Druckrückgewinnung in Oberschallkanälen," Deutsche Luftfahrtforschung, Forsch.Bericht Nr. 1756, 1943.

15 Starken, H., and Schimming, P., "Auswerteverfahren von zweidimensionalen Gittermessungen," DLR-Mitt, 72-03, 1972.

APPENDIX

Cascade geometries and experimental data:

1. DFVLR-SAV 16

1.1 Profile coordinates

(x-coordinate measured in chord-direction starting at the leading edge).

pressure side			suction side	
x		y	x	y
0.000	-	0.0000	0.000	0.0000
0.035	-	0.0009	0.035	0.0037
0.068	-	0.0018	0.069	0.0074
0.103	-	0.0027	0.104	0.0111
0.137	-	0.0037	0.139	0.0148
0.172	-	0.0046	0.174	0.0185
0.207	-	0.0055	0.208	0.0222
0.245	-	0.0065	0.243	0.0259
0.279	-	0.0073	0.278	0.0296
0.314	-	0.0080	0.313	0.0333
0.349	-	0.0085	0.347	0.0370
0.384	-	0.0089	0.382	0.0407
0.418	-	0.0091	0.417	0.0444
0.453	-	0.0093	0.450	0.0480
0.488	-	0.0092		
0.522	-	0.0091	corner	
0.557	-	0.0089		
0.592	-	0.0086	0.450	0.0480
0.627	-	0.0082	0.485	0.0472
0.661	-	0.0076	0.517	0.0462
0.696	-	0.0070	0.551	0.0450
0.731	-	0.0064	0.586	0.0435
0.765	-	0.0056	0.621	0.0415
0.800	-	0.0048	0.656	0.0392
0.835	-	0.0040	0.690	0.0366
0.870	-	0.0031	0.725	0.0336
0,904	-	0.0021	0.760	0.03o3
0.939	-	0.0012	0.794	0.0267
0.974	-	0.0001	0.829	0.0229
1.000	-	0.0000	0.864	0.0188
			0.899	0.0144
			0.933	0.0099
			0.968	0.0052
			1.000	0.0000

1.2 Cascade geometry

l = 130 mm

t/l = 0.348

β_s = 144 degree

design: M_1 = 2,0

β_1 = 139 degree.

1.3 Experimental data for β_1 = 139 degree, maximum back pressure

1.3.1 Point x

M_1	= 2,20	M_2	= 0.762
p_{t_1}	= 1.293'5 Pascal	p_{t_2}/p_{t_1}	= 0.781
p_1	= 0.1197'5 "	p_2/p_1	= 5.738
Re_1	= 1.7'6	AVR	= 1.47
		β_2	= 139.5 degree.

Loss coefficient profile $(p_{t_1} - p_{t_2})/(p_{t_1} - p_1)$,
(measured in equal steps over one pitch).

0.270	continued:
0.278	0.224
0.289	0.209
0.299	0.198
0.307	0.190
0.308	0.185
0.307	0.181
0.302	0.186
0.292	0.187
0.280	0.202
0.262	0.213
0.244	0.230
	0.244

1.3.2 Point △

M_1	= 2.30	M_2	= 0.820
p_{t_1}	= 1.184'5 Pascal	p_{t_2}/p_{t_1}	= 0.76
p_1	= 0.094'5 "	p_2/p_1	= 6.184
Re_1	= 1.6'6	AVR	= 1.592
		β_2	= 139.5 degree

Loss coefficient profile $(p_{t_1} - p_{t_2})/(p_{t_1} - p_1)$

0.199	continued:
0.199	0.379
0.201	0.381
0.204	0.373
0.208	0.356
0.204	0.333
0.212	0.310
0.236	0.281
0.271	0.252
0.311	0.226
0.344	0.204
0.368	0.185
	0.173

1.3.3 Point ⊙

M_1	= 2.36	M_2	= 0.800
p_{t_1}	= 1.075'5 Pascal	p_{t_2}/p_{t_1}	= 0.74
p_1	= 0.079'5 "	p_2/p_1	= 6.616
Re_1	= $1.4 \cdot 10^6$	AVR	= 1.595
		β_2	= 139.5 degree

Loss coefficient profile $(p_{t_1} - p_{t_2})/(p_{t_1} - p_1)$

0.170	continued:
0.185	0.396
0.205	0.378
0.232	0.349
0.257	0.313
0.289	0.278
0.319	0.254
0.349	0.235
0.373	0.227
0.391	0.227
0.401	0.232
0.405	0.248
	0.268

2. DFVLR-Tandem

2.1 Profile coordinates

chord length x	suction side y_{ss}	pressure side y_{ps}
0.00	0.000	0.000
0.05	0.023	0.018
0.10	0.044	0.036
0.15	0.065	0.050
0.20	0.086	0.064
0.25	0.106	0.075
0.30	0.124	0.085
0.35	0.139	0.092
0.40	0.149	0.096
0.45	0.156	0.099
0.50	0.160	0.101
0.55	0.161	0.099
0.60	0.159	0.097
0.65	0.153	0.092
0.70	0.143	0.085
0.75	0.130	0.077
0.80	0.113	0.065
0.85	0.092	0.052
0.90	0.066	0.036
0.95	0.035	0.018
1.00	0.000	0.000.

2.2 Cascade geometrie

First cascade: DFVLR-SAV 16
Second cascade: MCA

l_B	= 125 mm	b	= 18 mm
t/l_B	= 0.362	d	= 48 mm
β_{sB}	= 120.5 degree.		

2.3 Experimental data for β_1 = 139 degree, maximum back pressure

2.3.1 Point △

M_1	= 2.23	M_2	= 0.563
p_{t_1}	= 1.182'5 Pascal	p_{t_2}/p_{t_1}	= 0.719
p_1	= 0.105'5 "	p_2/p_1	= 6.529
Re_1	= $2.1 \cdot 10^6$	AVR	= 1.729
		β_2	= 95 degree

Loss coefficient profile $(p_{t_1} - p_{t_2})/(p_{t_1} - p_1)$

0.328	continued:
0.356	0.301
0.378	0.292
0.390	0.288
0.396	0.285
0.398	0.281
0.391	0.277
0.381	0.269
0.364	0.257
0.346	0.246
0.328	0.240
0.313	0.253
	0.258

2.3.2 Point ⊙

M_1	= 2.34	M_2	= 0.573
p_{t_1}	= 1.276'5	p_{t_2}/p_{t_1}	= 0.658
p_1	= 0.952'5	p_2/p_1	= 7.064
Re_1	= 2.1'6	AVR	= 1.764
		β_2	= 95 degree.

Loss coefficient profile $(p_{t_1}-p_{t_2})/(p_{t_1}-p_1)$

0.374	continued:
0.380	0.380
0.412	0.375
0.434	0.366
0.447	0.358
0.452	0.350
0.448	0.346
0.439	0.330
0.428	0.316
0.417	0.293
0.408	0.283
0.399	0.286
0.387	

2.3.3 Point +

M_1	= 2.40	M_2	= 0.574
p_{t_1}	= 1.218'5 Pascal	p_{t_2}/p_{t_1}	= 0.630
p_1	= 0.084'5 "	p_2/p_1	= 7.322
Re_1	= 2.0'6	AVR	= 1.787
		β_2	= 96 degree

Loss coefficient profile

0.395	continued
0.425	0.408
0.448	0.400
0.461	0.393
0.465	0.383
0.464	0.371
0.461	0.356
0.453	0.344
0.444	0.331
0.436	0.323
0.428	0.330
0.420	0.363
0.413	

3. DFVLR-SAV 21

3.1 Profile coordinates

pressure side		suction side	
x	y	x	y
0.000	0.000	0.000	0.000
0.039	0.013	0.039	0.020
0.074	0.025	0.078	0.039
0.114	0.039	0.118	0.059
0.153	0.052	0.157	0.079
0.197	0.067	0.196	0.099
0.236	0.080	0.235	0.118
0.275	0.092	0.274	0.138
0.315	0.104	0.317	0.157
0.354	0.114	0.352	0.169
0.393	0.123	corner	
0.432	0.130		
0.471	0.135	0.352	0.169
0.511	0.138	0.391	0.181
0.550	0.138	0.431	0.191
0.589	0.137	0.470	0.198
0.628	0.134	0.509	0.202
0.667	0.128	0.548	0.202
0.707	0.120	0.587	0.199
0.746	0.110	0.627	0.193
0.785	0.098	0.666	0.184
0.824	0.084	0.705	0.172
0.863	0.068	0.744	0.156
0.903	0.051	0.783	0.139
0.942	0.032	0.823	0.118
0.981	0.011	0.862	0.096
1.000	0.000	0.901	0.071
		0.940	0.044
		0.979	0.016
		1.000	0.000

3.2 Cascade geometrie

l = 100 mm

t/l = 0.26

β_s = 125 degree.

3.3 Experimental data for β_1 = 139 degree, maximum back pressure

3.3.1 Point ⊙

M_1 = 2.27 M_2 = 0.703

p_{t_1} = 1.189'5 Pascal p_{t_2}/p_{t_1} = 0.710

p_1 = 0.099'5 " p_2/p_1 = 6.149

Re_1 = 1.6'6 AVR = 2.01

β_2 = 94°

Loss coefficient profile $(p_{t_1}-p_{t_2})/(p_{t_1}-p_1)$

0.419	continued
0.428	0.237
0.415	0.252
0.410	0.285
0.411	0.306
0.382	0.335
0.357	0.364
0.312	0.381
0.295	0.398
0.261	0.417
0.233	0.434
0.224	
0.215	
0.214	

3.3.2 Point ▽

M_1	= 2.30	M_2	= 0.634
p_{t_1}	= 1.217'5 Pascal	p_{t_2}/p_{t_1}	= 0.657
p_1	= 0.095'5 "	p_2/p_1	= 6.406
Re_1	= 1.6'6	AVR	= 1.81
		β_2	= 97 degree

Loss coefficient profile $(p_{t_1}-p_{t_2})/(p_{t_1}-p_1)$

0.282	continued
0.292	0.457
0.305	0.448
0.317	0.440
0.353	0.402
0.378	0.389
0.395	0.353
0.420	0.332
0.429	0.299
0.438	0.305
0.448	0.301
0.456	
0.460	
0.458	

3.3.3 Point ⊡

M_1	= 2.40	M_2	= 0.637
p_{t_1}	= 1.273'5 Pascal	P_{t_2}/p_{t_1}	= 0.623
p_1	= 0.087'5 "	p_2/p_1	= 6.926
Re_1	= 1.6'6	AVR	= 1.81
		β_2	= 94 degree

Loss coefficient profile $(p_{t_1}-p_{t_2})/(p_{t_1}-p_1)$

0.489
0.497
0.502
0.505
0.506
0.496
0.486
0.477
0.456
0.439
0.402
0.383
0.360
0.330
0.316
0.309
0.310
0.332
0.355
0.385
0.415
0.446
0.470
0.490